PETPVC: A toolbox for performing partial volume correction techniques in positron emission tomography

Benjamin A. Thomas[1,2], Vesna Cuplov[2], Alexandre Bousse[2], Adriana Mendes[3], Kris Thielemans[2], Brian F. Hutton[2,4], Kjell Erlandsson[2]

[1]Agency for Science Technology and Research - National University of Singapore Clinical Imaging Research Centre, Singapore

[2]Institute of Nuclear Medicine, University College London Hospital, University College London, London, UK

[3]Institute of Biophysics and Biomedical Engineering, Faculty of Science, University of Lisbon, Portugal

[4]Centre for Medical Radiation Physics, University of Wollongong, New South Wales, Australia

Corresponding author:

Benjamin A. Thomas, PhD

A*STAR-NUS Clinical Imaging Research Centre

National University of Singapore Centre for Translational Medicine

14 Medical Drive - #B1-01

Singapore 117599

Tel: +65 6601 3904

E-Mail: Benjamin_Thomas@circ.a-star.edu.sg

Running title: PET partial volume correction toolbox

Keywords: partial volume correction, positron emission tomography, partial volume effects, PET/MR

Word count: 7520 words

Abstract

Positron emission tomography (PET) images are degraded by a phenomenon known as the partial volume effect (PVE). Approaches have been developed to reduce PVEs, typically through the utilisation of structural information provided by other imaging modalities such as MRI or CT. These methods, known as partial volume correction (PVC) techniques, reduce PVEs by compensating for the effects of the scanner resolution, thereby improving the quantitative accuracy. The PETPVC toolbox described in this paper comprises a suite of methods, both classic and more recent approaches, for the purposes of applying PVC to PET data.

Eight core PVC techniques are available. These core methods can be combined to create a total of twenty-two different PVC techniques. Simulated brain PET data are used to demonstrate the utility of toolbox in idealised conditions, the effects of applying PVC with mismatched point-spread function (PSF) estimates and the potential of novel hybrid PVC methods to improve the quantification of lesions.

All anatomy-based PVC techniques achieve complete recovery of the PET signal in cortical grey matter (GM) when performed in idealised conditions. Applying deconvolution-based approaches results in incomplete recovery due to premature termination of the iterative process. PVC techniques are sensitive to PSF mismatch, causing a bias of up to 16.7% in GM recovery when over-estimating the PSF by 3mm. The recovery of both GM and a simulated lesion was improved by combining two PVC techniques together.

The PETPVC toolbox has been written in C++, supports Windows, Mac and Linux operating systems, is open-source and publicly available.

1. Introduction

The quantification of positron emission tomography (PET) imaging is affected by the partial volume effect (PVE), caused by the finite spatial resolution of the scanner. The reconstructed PET image resolution is limited by several factors, namely, the positron range of the radionuclide being imaged, detector size, non-colinearity of annihilation photon pairs and the chosen reconstruction parameters. These factors result in an image resolution that is around 5 to 6 mm full-width at half maximum (FWHM) for a typical whole-body PET scanner. The limited spatial resolution results in a blurring of the image, altering the apparent position of activity. It is this displacement that causes degradation in the accuracy of quantitative assessment.

PVE is a term used to describe two phenomena that degrade the quantitative accuracy of PET data. The first is the aforementioned blurring due to the scanner resolution. The second effect is due to the voxel grid used to sample the image. A given voxel can contain multiple tissue types, with the resulting voxel value representing the average signal from these fractional contributions. The mean signal does not necessarily represent the true distribution of the radiotracer accurately. This averaging of the signal intensity within a voxel is referred to as the *tissue-fraction effect* and also affects quantification.

Partial volume correction (PVC) methods have been proposed which reduce PVEs by compensating for the effects of resolution on the PET data, thereby improving the quantitative accuracy of the images. PVC techniques can either be included within the PET reconstruction or applied as a post-reconstruction step. Within-reconstruction PVC is often referred to as resolution recovery (RR). This must be supported by the scanner manufacturer, or in a research context, requires fully quantitative offline reconstruction software, which is not easily obtainable. Offline reconstructions need listmode or sinogram data. These data are not often available outside of a research setting. This paper focuses on software for post-reconstruction PVC methods that can be applied to both research and clinical data using existing reconstructed images.

PVC approaches can be either purely data-driven or utilise additional structural information from other imaging modalities such as magnetic resonance imaging (MRI) or computed tomography (CT), see Erlandsson et al. for an extensive review [1], [2]. The severity of PVEs is dependent on the size of the object being measured, with smaller structures being affected more than larger ones [3]. PVEs will affect the maximum intensity value of any structure that is smaller than 2.5-3 times the FWHM of the scanner [4].

PVC techniques require an accurate measure of the point-spread function (PSF) of the scanner. Although the scanner PSF varies with position within the PET field-of-view, when applying PVC, the PSF is usually approximated by a spatially-invariant Gaussian kernel [5], [6]. While this simplification may not be appropriate for whole-body imaging, this assumption is generally accepted when applying PVC to brain PET data.

The cortex is commonly of interest when performing human brain PET imaging. As the cortex is at most a few mm thick, cortical structures tend to be severely affected by PVEs. This is a particular issue when assessing neurodegenerative diseases such as Alzheimer's disease (AD) where atrophy can cause extensive losses in cortical grey matter volume. In this context, apparent signal changes can be at least partially attributed to PVEs [7], [8]. Correcting for these PVEs may be beneficial, especially when studying longitudinal change [9]. However, there are still concerns about the sensitivity of PVC techniques to registration and segmentation errors, with no firm consensus as to which approach is the best to take [3], [10]. The toolbox described in this paper can be used to address these questions.

Efforts to develop PVC software have been previously reported. PVELab [11] is a MATLAB-based (Mathworks, Natick, M.A., USA) toolbox that provides both voxel-based and region-based PVC techniques. Volumes of interest (VOIs) can be propagated from the Hammers atlas, or from another source, for the purpose of applying the Geometric Transfer Matrix (GTM) method [12], amongst others. Similarly, PMOD (PMOD Technologies Ltd., Zurich, Switzerland) - a proprietary application - performs GTM as well as a classical Müller-Gärtner (MG), utilising the

Hammers' atlas [13]. Shidahara et al. released the Structural-Functional Synergistic Resolution Recovery (SFSRR) method as a MATLAB software tool [14]. Most recently, Chonde et al. [15] proposed a MATLAB user interface – Masamune – to a data-processing pipeline which incorporates PVC for dynamic PET analysis, as part of a brain PET-MR workflow.

In this paper the PETPVC toolbox is presented, which is open-source and comprises a suite of methods for performing PVC on PET data. It aims to encourage adoption of existing approaches and facilitate research in this field. All provided techniques are capable of correcting for the tissue-fraction effect where appropriate data are available. Eight core methods are provided: MG, the GTM method, region-based voxel-wise correction (RBV), the Labbé method (LAB), multi-target correction (MTC), iterative Yang (IY) and the reblurred Van-Cittert (RVC) and Richardson-Lucy (RL) deconvolution techniques. Certain combinations of these core methods can then be compounded to create a total of twenty-two different approaches.

PETPVC has been written in C++ using the Insight Segmentation and Registration Toolkit (ITK) [16]. Each correction method has been implemented as an ITK filter to facilitate pipeline processing. The toolbox supports Windows, Mac and Linux operating systems. The PETPVC toolbox has been made open-source under an Apache version 2.0 license and is publicly available on GitHub (https://github.com/UCL/PETPVC).

2. Methods

2.1 PVC techniques

The toolbox implements eight core post-reconstruction PVC techniques. The MG and GTM approaches, two classic PVC methods that are so far most commonly applied, are provided. In addition, LAB and the more recently proposed MTC, RBV and IY correction are available. Two deconvolution techniques, RVC and RL, are also included. While most techniques have been described elsewhere, below is a brief description of each method.

2.1.1   Müller-Gärtner (MG)

The MG technique [13] utilises a patient-specific, registered MRI that is segmented into three tissue classes; grey matter (GM), white matter (WM) and cerebro-spinal fluid (CSF). Ordinarily a T1-weighted, high resolution image (voxel size $\leq$ 1mm^3) is used for the purposes of segmentation. The MG approach corrects one tissue compartment, in most instances the GM, on a voxel-by-voxel basis. MG corrects for PVE by scaling the other tissue classes by an estimate of the average activity in that compartment, convolving these estimates by the scanner PSF and subtracting them from the original PET image. This removes the spilled-in activity of these regions from the GM. The resultant image is then divided by the GM tissue mask, which has been convolved by the PSF, on a voxel-by-voxel basis to correct for PVEs in GM. The final image contains GM voxels only. MG assumes that the WM and CSF compartments can be accurately described by their mean values which are typically found by eroding the respective tissue masks to avoid GM spill-over effects. The contribution from CSF is normally considered to be zero and so correction for the CSF compartment is usually omitted, as it has been in PETPVC.

2.1.2   Geometric Transfer Matrix (GTM)

The GTM method [12] is a VOI-based method that uses parcellated MRI data to correct for multiple compartments simultaneously. Activity in each of the n VOIs is assumed to be uniform. The mean activity for each region is measured from the observed PET image and stored in a

vector **r**, where **r** = [r$_{1,…,}$r$_n$]. The GTM (G) is a matrix of size $n \times n$ containing the fractional contribution (spill-over) of activity from one region into another. The fractional contribution ($G_{j,i}$) of region R_j into region R_i is calculated by smoothing the region R_j by the PSF, multiplying it by region R_i and calculating the sum of the remaining voxels, normalised by the sum of R_i. When the fractional contributions of all regions into all others have been computed, the true activity values (T) can be found by applying: $T = G^{-1}r$. The resulting vector will contain the PV-corrected mean value for each region. The GTM approach assumes that the activity within a region is uniform and can be accurately described by its mean value. Also, the technique does not produce an image so is only appropriate when average VOI activity values are solely of interest. When defining the regions to be used with the GTM approach, it is necessary to ensure that all potential sources of spill-over that could affect a region of interest (ROI) are taken into account during correction. Therefore when applying GTM to assess cortical ROIs, it is generally appropriate use a set of regions that cover the whole brain. The PETPVC toolbox permits any region definition that the user feels is suitable for their particular application.

2.1.3 Labbé (LAB)

The Labbé approach [17] is also a VOI-based method. Corrected regional mean values are found using a matrix inverse, as in the GTM approach described above. However, the LAB method differs in the way that the spill-over and uncorrected values are calculated. Both regions R_j and R_i are convolved with the scanner PSF when estimating the fractional contribution of R_j into R_i. In addition, the estimate of the uncorrected regional mean of r_i is calculated over $R_i \otimes h$, where h is the scanner PSF, $\otimes$ is a 3D convolution operator. These seemingly subtle differences result in a different bias vs. noise trade-off compared to the GTM method.

2.1.4 Multi-target correction (MTC)

The MTC method [18] is a hybrid PVC technique performing both VOI- and voxel-based corrections. First, estimates of regional mean values are calculated using the GTM method. A

voxel-wise correction is then performed for multiple regions. The voxel-wise correction is performed as follows:

$$f_C(x) = \sum_{j=1}^{n} p_j(x) \frac{f(x) - \sum_{i \neq j} T_i p_i(x) \otimes h(x)}{p_j(x) \otimes h(x)} \tag{1}$$

where f_C is the PV-corrected image, f is the observed image, p_i and p_j are the masks of regions R_i and R_j respectively and T_i is the corrected mean value of R_i calculated using the GTM. Essentially, each region is in turn considered to be the target region (for correction) while all other regions are treated as neighbouring regions. The mean value estimate is used for the neighbouring regions only, while the observed PET image values are used in the target region. Unlike MG, GTM and LAB, MTC produces a corrected image for all regions which can then be used for voxel-based analysis.

2.1.5 Region-based voxel-wise correction (RBV)

RBV correction [19] is an extension of the previously described GTM method and the voxel-wise correction of Yang et al. [20]. The mean VOI activity values are calculated using the GTM, then a voxel-by-voxel correction is performed in order to produce a corrected image. To compute the voxel-wise correction a 'synthetic' image is created using the GTM-calculated mean values: $s(x) = \sum_{i=1..n}[T_i p_i(x)]$, where T_i is the PV-corrected mean value of region R_i, and $p_i(x)$ is the probability that the voxel at location x belongs to R_i ($p(x) = 1$, when completely inside; $p(x) = 0$, when completely outside). The voxel-wise correction [20] is then applied by:

$$f_C(x) = f(x) \left[\frac{s(x)}{s(x) \otimes h(x)} \right] \tag{2}$$

where f is the observed PET image, h is the scanner PSF, $\otimes$ is a 3D convolution operator and f_c is the corrected image. The difference between RBV correction and MTC is that here all regions are corrected simultaneously rather than the target/neighbour approach of MTC.

2.1.6 Iterative Yang (IY)

The IY technique [1] is a further adaptation of the Yang method. Instead of calculating the regional mean values via the GTM, the values are estimated from the PET data itself. The Yang correction is applied and the mean value estimates are recalculated. This process is iterated several times by the iterative scheme is given below:

$$f_{k+1}(x) = f(x) \left[\frac{s_k(x)}{s_k(x) \otimes h(x)} \right],$$

$$s_k(x) = \sum_{i=1..n} [T_{k,i} p_i(x)],$$

$$T_{k,i} = \frac{1}{v_i} \left[\sum_{j \in p_i} f_{k,j} \right],$$

$$f_0 = f.$$

(3)

where f is the observed PET image, p_i is the mask of region R_i, v_i is the number of voxels in region R_i and $T_{k,i}$ is the estimated mean value of R_i at iteration k. The image s_k is a piece-wise constant image of the average values for each region and f_k is the estimate of the PV-corrected image at iteration k. The execution of IY is generally faster than RBV (and GTM) as k convolutions are performed with IY, where k is normally less than ten. When performing RBV, n convolutions are computed, where n is the number of VOIs. However, the resulting image is close to that of RBV [10].

The formulation presented above requires piece-wise constant region definitions and an additional step is necessary before the voxel-wise correction is applied to regions that contain tissue-fraction information. This extra stage is referred to as 'fuzziness correction'. The mean values (T) for each region are weighted according to how smooth each region mask is in relation to every other region. Conceptually, these weights are calculated in the same way as the GTM, while omitting the convolution by the PSF. The region weights are stored in a matrix (W) of size $n \times n$. The weight of region $w_{i,j}$ is calculated by:

$$w_{i,j} = \frac{\sum_x p_i(x)p_j(x)}{\sum_x p_i(x)}. \tag{4}$$

The 'fuzziness correction' is then applied to the current estimate of the regional mean values by inverting W:

$$M = W^{-1}T \tag{5}$$

Thus the IY correction then becomes:

$$f_{k+1}(x) = f(x)\left[\frac{s_k(x)}{s_k(x) \otimes h(x)}\right],$$

$$s_k(x) = \sum_{i=1..n} \left[M_{k,i}p_i(x)\right],$$

$$M_{k,i} = W^{-1}T_{k,i}, \tag{6}$$

$$T_{k,i} = \frac{1}{v_i}\left[\sum_{j \in p_i} f_{k,j}\right],$$

$$f_0 = f.$$

2.1.7 Deconvolution techniques

The PVC methods described above are all based on anatomical images, which have been segmented/parcellated into a number of regions. These methods correct for PVEs that correspond to spill-over of data from one region to another (inter-regional PVEs). They do not correct for PVEs between voxels within the same region (intra-regional PVEs). Various deconvolution techniques can be used to reduce the effect of blurring, without the need for segmentation. The level of correction achievable with these techniques is limited and they also lead to noise-amplification in the image. However, they can be useful for improving the definition of image features, for which no corresponding segmentation is available. Deconvolution can be used for intra-regional PVC as an extension to voxel-based inter-regional PVC algorithms.

The classic RL and RVC deconvolution techniques have been implemented in the toolbox [21], modified in such a way that they can be applied to individual regions. Both techniques are based on iterative algorithms. The RL technique assumes a Poisson noise model and is based on a multiplicative correction step, while the RVC technique assumes a Gaussian noise model and is based on an additive correction step. The original algorithms can be described as follows [21]:

$$f_{k+1}(x) = f_k(x) \left[h(x) \otimes \frac{f(x)}{h(x) \otimes f_k(x)} \right];$$

(7)

for the RL technique and

$$f_{k+1}(x) = f_k(x) + \alpha \cdot h(x) \otimes [f(x) - h(x) \otimes f_k(x)];$$

(8)

where α is the step-size, for the RVC method. Both algorithms are initialised with $f_0(x) = f(x)$.

In order to use these techniques for intra-regional PVC of a region of R_i, a voxel-based inter-regional PVC method is first applied to the images, and then followed by a modified version of one of the deconvolution algorithms above, where each convolution is replaced by the following operation:

$$X_{p_i,h}: f(x) \longmapsto p_i(x) \frac{[p_i(x)f(x)] \otimes h(x)}{p_i(x) \otimes h(x)} + (1 - p_i(x))f(x)$$

(9)

where $p_i(x)$ is the mask of region R_i (with values of 0 or 1).

The intra-regional deconvolution algorithms can then be described as follows:

$$f_{i,k+1}(x) = f_{i,k}(x) \left[X_{p_i,h} \left(\frac{f(x)}{X_{p_i,h} f_{i,k}(x)} \right) \right]$$

(10)

and

$$f_{i,k+1}(x) = f_{i,k}(x) + \alpha \cdot X_{p_i,h} [f(x) - X_{p_i,h} f_k(x)]$$

(11)

11

These corrections can be applied to a single region or to multiple regions.

2.1.8 Hybrid methods

From the eight core algorithms provided, it is possible to create fourteen additional PVC techniques by using them in combination. For example, the MG technique could first be applied to correct for spill-over between GM and WM, followed by an RVC deconvolution, constrained to the GM, to reduce PVE between GM regions. This technique is referred to as MG-RVC. Similarly, while RBV correction was originally proposed using the GTM approach to estimate regional means, it is possible to use LAB instead, resulting in LAB-RBV. Figure 1 shows how the additional fourteen hybrids can be formulated from the eight core methods.

Figure 1 here

2.2 Description of the software

The PETPVC toolbox consists of the 22 PVC techniques described in the previous section. The techniques are provided as a library of ITK filters[1], and a set of command-line applications conforming to the Slicer execution model [22]. The filters can either be incorporated into existing processing pipelines or run through the command-line applications provided. Each application consists of a main function that handles image file I/O and user-specified parameters. The appropriate PVC filter is then configured and executed, with the results being written back to the output file(s). The command-line applications can be run from both 3D Slicer and the Medical Imaging Interaction Toolkit (MITK) [23], [24].

All methods in the toolbox require the PET imaging data and segmented structural information (with the exception of RL and RVC when applied in isolation) to be provided in an imaging format that can be read by the ITK file reader class. The possible input file types include: NifTI,

---

[1] It is recommended to build the toolbox with ITK v.4.7 or newer as this supports large NifTI files.

compressed NifTI, Analyze, ITK MetaImage and NRRD. The user needs to ensure that the PET data is appropriately converted from DICOM to a suitable input file type[2].

In total there are currently ten applications in the toolbox: *pvc_mg*, *pvc_gtm*, *pvc_labbe*, *pvc_mtc*, *pvc_rbv*, *pvc_iy*, *pvc_diy*, *pvc_vc*, *pvc_rl* and *petpvc*. The first six implement the MG, GTM, LAB, MTC, RBV and IY corrections respectively, all with the ability to also correct for tissue-fraction effect when supplied with appropriate segmentations. *pvc_diy*, or 'discrete IY' is a version of IY dedicated to processing 3D region mask images that contain piece-wise constant labels. This additional application has been provided to facilitate PVC potentially using hundreds of VOIs. The RVC and RL methods are executed using *pvc_vc*, *pvc_rl* respectively and do not require structural information as they operate from the PET data alone. The final application, *petpvc*, can execute all of the available core and hybrid PVC methods.

2.3   Testing framework

To ensure the correct functionality of the PVC algorithms, automatic testing can be performed. Scripts are provided as part of the PETPVC toolbox that check the function of the PVC methods. CTest, part of the CMake package, is a testing tool that is used to execute the test scripts. The testing procedure consists of smoothing simulated test objects and then PV-correcting these data. The VOI values in the corrected data are validated against the expected VOI values.

2.4   Region definitions

A key input to the PVC methods is the file containing the VOI definitions. These can either be binary or represent tissue-fractions. The applications, with the exception of *pvc_diy*, assume that the file is a 4D volume, where each 3D volume represents a single segmented region. The use of 4D volumes facilitates the processing of tissue-fraction segmentations, allowing the tissue-fraction effect to be taken into account as part of the correction. All voxel values (x) within a 3D

---

[2] ITK provides example code for such conversions.

volume must be in the range $0 \leq x \leq 1$. The sum across the 4th dimension should also be equal to 1, requiring the background (the area outside the head) to also be included as a segmented region.

In the case of *pvc_diy*, a single 3D volume of discrete unsigned integers - one per region - is required. The values do not need to be contiguous and any voxel with a value of 0 is assumed to be part of the background.

3. Materials

Example results of the PVC toolbox applications are demonstrated using data simulated to represent 18F-Fludeoxyglucose (FDG) and 11C-Pittsburgh compound B (PIB) brain PET studies. First, the techniques' performance are evaluated for the FDG simulation in idealised conditions, i.e. there are no registration or segmentation errors and the PSF for simulation and correction are exactly matched. Second, the effect of PSF mismatch is demonstrated. Finally, an example of the potential application of one of the hybrid methods, RBV-RVC, is reported. The corrections and their effect on commonly used reference regions for PIB, cerebellar grey matter and sub-cortical WM, are subsequently demonstrated.

3.1   Noise-free data simulation

A T1-weighted MP-RAGE scan of a healthy volunteer, with a resolution of 1x1x1 mm^3 was segmented with the Geodesic Information Flows (GIF) framework [25]. The resulting GM, WM and CSF segmentations (3-class) were used for subsequent processing.

3.1.1   FDG

An FDG-like PET distribution was created, referred to as the ground truth (GT), for evaluating PVC performance. This was created by applying a GM:WM:CSF ratio of 4:1:0. To simulate the reconstructed PET resolution, a 6mm (FWHM) 3D Gaussian smoothing was applied to the GT. No statistical noise was added to the simulations.

For the purposes of demonstrating the RBV-RVC correction, a 1cm diameter sphere was added in the sub-cortical WM of the GT image to represent a lesion. The lesion was given the value of 3 and the image was then smoothed with the same 6mm kernel.

3.1.2   PIB

A PIB-like PET distribution simulating an AD patient with high amyloid burden was created from the parcellation provided by GIF. The PIB distribution was created from a total of 42 brain regions

covering cerebellar GM, cerebellar WM, CSF, pons, brain stem, sub-cortical WM, frontal, parietal, temporal, occipital and sub-cortical GM structures. To model a PIB distribution with an AD-like appearance, voxels in cortical regions commonly affected by the disease were given values between 1.5 and 3 times higher than cerebellar GM. The precuneus had the highest value of 3 relative to the cerebellum. The CSF was assumed to have zero uptake. As with the FDG simulation, a 6mm Gaussian smoothing was applied to the GT PIB distribution to produce a PET-like image.

3.2   Monte Carlo PIB simulation

In order to generate simulated data that are more realistic in terms of noise, Monte Carlo simulations were performed for two different PIB distributions. The MP-RAGE scans of a healthy volunteer (HV) without severe cortical atrophy, and an AD patient with cortical atrophy, were acquired using a Siemens Biograph mMR (Siemens Healthineers, Erlangen, Germany). These subsequently were parcellated as described previously. A low PIB distribution was created using the parcellation of the HV. A high distribution was generated from the AD patient data.

In addition to the MP-RAGE, ultra-short echo time (UTE) images were acquired for the purposes of MR-based attenuation correction (MRAC). The attenuation maps were used for the purpose of simulating the effects of attenuation and attenuation correction. The surrounding head and neck tissue, nasal cavities and skull were added to the subject distributions. Monte Carlo simulations were performed using a model of the mMR in PET SORTEO [26]. A 30 minute scan representing an acquisition at 40-70 minutes post-injection was simulated. Ten noise realisations were performed for each distribution. These data were then reconstructed using JSRecon and e7tools, provided by Siemens. All reconstructions were performed using Ordinary-Possion Ordered-Subset Expectation Maximisation (OP-OSEM) with 4 iterations and 21. The matrix size was $344 \times 344 \times 127$ with a voxel size of $2.09 \times 2.09 \times 2.03$ mm. A 2 mm Gaussian post-filter was applied. The reconstructed images were then resampled to the MR matrix size in order to apply PVC.

3.3   Partial volume correction and analysis of FDG data

First, the performance of the techniques is assessed in an idealised situation for all methods (i.e. when the segmentations exactly match the simulated distribution). The eight core PVC techniques (MG, GTM, LAB, MTC, RBV, IY, RVC and RL) are applied to PET image, using the 3-class segmentations where anatomical information is required. RVC is performed using the suggested parameters of Tohka et al. [19] (α=1.5; maximum of 30 iterations; stopping criterion = 0.01). RL is executed for 10 iterations. Both RVC and RL need to be halted before full recovery can be achieved due to noise amplification issues [21]. The mean recovery coefficient (RC) for GM and WM are reported. Second, the effect of PSF mismatch is demonstrated by performing PVC for all methods with under- and over-estimated values of the PSF ($\pm$3mm). The mean RC is reported for the GM region. Third, the simulated data with added lesion is evaluated for the hybrid RBV-RVC approach and the core voxel-based techniques which can correct for multiple tissue compartments (MTC, RBV, IY, RVC and RL). The methods that require anatomical information are provided with the original 3-class segmentation. This means the location of the lesion is absent in the structural data. The mean RC ($\pm$ s.d.) is reported for the lesion.

3.3.1   Recovery coefficient calculation

The RC is defined as the ratio of the PV-corrected image to the GT. Mean RC values were calculated by dividing each PV-corrected image by the associated GT and then taking the mean of regions defined by the segmentation.

3.4   Partial volume correction and analysis of noise-free PIB data

All eight core techniques are applied to the PIB PET image. The 42 region parcellation is provided for the purposes of PVC. In the case of MG, the 3-class segmentation is used. The PV-corrected images are subsequently normalised by the mean of 1) the cerebellar GM and 2) the sub-cortical WM to create standardised uptake value ratio (SUVR) images. A composite cortical SUVR value

is calculated from the average of the mean SUVRs in the frontal, parietal, temporal, occipital and precuneus regions. These composite SUVRs are reported for both reference regions.

3.5   Partial volume correction and analysis of Monte Carlo simulated PIB data

All eight core techniques are applied to simulations of both the HV and AD subject, for each noise realisation. The 42 region parcellation is provided for the purposes of PVC. As described previously, a 3-class segmentation is used for the MG correction. The PV-corrected images are subsequently normalised by the mean of the cerebellar GM to create SUVR images. Mean composite cortical SUVRs across noise realisations are reported for both PIB distributions.

4. Results

Trans-axial slices of the GT, simulated PET and the PV-corrected data, for those techniques that produce images, can be seen in figure 2. The mean RC calculated for each of the eight methods is shown in figure 3. Without PVC there is an average 34% underestimation of the GM and 83% over-estimation of WM. After PVC, all anatomy-based methods achieve either perfect (RC=1) or near perfect recovery, for both the GM and WM compartments. The performance of the deconvolution techniques, RVC and RL, is poorer than the other approaches. In GM, RVC and RL achieve a RC of 0.74 and 0.78 respectively. The WM also remains over-estimated when applying the deconvolution approaches.

Figure 2 and 3 here

Figure 4 shows the effect that PSF mismatch has on the RC of GM. An overestimation of 1mm results in a positive bias of between 2.8% (LAB) and 5.5% (RBV) for the anatomy-based methods. At 3mm, the bias increases to between 7.4% (LAB) and 16.7% (RBV). The deconvolution techniques always under-correct (RC < 1) the GM, even when the PSF is overestimated.

Figure 4 here

The simulated lesion images and RBV, RVC and RBV-RVC corrected images can be seen in figure 5. Mean RC values of the lesion (figure 6) demonstrates that no technique achieves complete recovery in the lesion. Higher RC values were observed with the deconvolution approaches, RVC (0.81) and RL (0.86), but they visibly underestimate GM. The anatomical techniques of RBV, MTC and IY do not improve recovery of the lesion with mean RC values of 0.61, 0.64 and 0.61 respectively. However, the GM recovery is accurate. The hybrid RBV-RVC method has both accurate GM recovery and the increased RC in the lesion (0.80), similar to of RVC.

Figure 5 and 6 here

A sagittal slice through the noise-free PIB GT and PET images is shown in figure 7. The mean composite cortical SUVRs for each technique, with both reference regions, are presented in figure 8. Without PVC the measured SUVR was 26.8% lower than the GT. After PVC and normalisation to cerebellar GM, RBV, IY, MTC, GTM and LAB all achieve complete recovery. MG was 7.6% lower than the GT. The deconvolution techniques, RVC and RL were 21.5% and 18.5% lower respectively. When sub-cortical WM was used as the reference region, a negative bias of 32.9% was observed before PVC. IY was 2.8% lower than the GT when sub-cortical WM was used for normalisation. RVC and RL were 29.5% and 25.9% lower than the GT.

Figure 7 and 8 here

The original subject MR image, GT distribution and Monte Carlo simulated data of the HV and AD subject are shown in figure 9. Mean composite cortical SUVRs, across noise realisations, are given in figure 10. For the AD simulation, the mean measured SUVR was 1.9 ± 0.2 before PVC ($-30.9 \pm 10.1\%$ compared to the GT). Increases in mean SUVR we observed for each of the PVC techniques. The anatomy-based methods were all within 10% of the GT SUVR. Of these, LAB was the most accurate with a mean SUVR of 2.6 ± 0.2 ($-3.5 \pm 7.6\%$). The MG correction was the poorest of the anatomy-based methods with a SUVR of 2.5 ± 0.3 ($-9.9 \pm 12.2\%$). The SUVRs for RVC and RL were 2.2 ± 0.4 ($-19.1 \pm 18.2\%$ and $-18.8 \pm 16.7\%$ respectively).

Without PVC, the mean SUVR for the HV simulation was 1.4 ± 0.1 ($14.8 \pm 8.6\%$ higher than the GT). After PVC, reductions in composite SUVRs were observed for all methods. The means observed for the anatomy-based methods were all within 3% of the GT. Although the SUVRs reduced for both RVC and RL, the standard deviations also increased when applying these techniques.

Figure 9 and 10 here

5. Discussion

The core PVC techniques of the toolbox have been demonstrated in idealised conditions with simulated data. The anatomy-based PVC techniques achieve complete recovery of the PET distribution. This is to be expected as there are no registration and segmentation errors or noise (other than the smoothing) in the simulated PET image. However, despite these conditions, the data-driven deconvolution-based approaches tended to under-correct when applied using the selected parameters. While during this noiseless simulation it would have been possible to perform larger numbers of iterations and therefore achieve higher recovery, the parameters were used in order to give the reader an indication of the typical performance of these approaches.

The sensitivity to PSF mismatch of the core techniques has been evaluated by applying PVC with under- and over-estimates of the smoothing kernel. Of the anatomy-based methods, the Labbé technique appears to be least sensitive to PSF mismatch, while the GTM-based approaches (GTM itself, RBV and MTC) were more sensitive. The toolbox provides the ability to combine both Labbé and RBV which may provide both the robustness of the Labbé approach, along with a voxel-wise correction. All the PVC technique are sensitive to PSF mismatch, and it is important to establish a realistic estimate of the PSF before attempting to apply PVC.

The core correction techniques were demonstrated with simulated PIB data for two different reference regions. The methods which account for all compartments accurately correct for the PVE, irrespective of normalisation approach. The small negative bias in SUVR observed with IY when using the sub-cortical WM was due to reference region being slightly positively biased compared to the GT. The MG can be affected by spill-over between GM regions as well as biases induced by the estimate of WM uptake [19]. This is pertinent when white matter reference regions such as sub-cortical WM, brain stem, pons or the corpus callosum are to be used. The reference region itself may be affected by PVEs due to the high and variable GM signal in patient populations. The MG technique assumes uniform uptake within a compartment and does not

apply PVC to the WM. As a result, it is not recommended to apply the MG approach to amyloid PET data.

The core PVC techniques have also been evaluated using Monte Carlo simulated PIB data for both a healthy and AD subject. The effects of PVC are more dramatic when applied to the AD case. This is to be expected as AD subjects tend to have a greater degree atrophy and therefore cortical regions are more severely partial volume effected. A reduction in cortical SUVR values was observed for the HV simulations. This reduction is due to the correction for WM spill-over effects. As was the case with the noise-free simulations, the deconvolution-based techniques performed more poorly than the anatomy-based approaches. These methods are known to amplify noise and it is necessary to terminate their execution prematurely, resulting in incomplete recovery.

A potential application of the hybrid RBV-RVC technique has been demonstrated using a simulated spherical lesion. These hybrids may provide at least partial PVC in regions when no anatomical information is available or where the appropriate segmentation is unclear. RBV-RVC was shown to provide both accurate correction where anatomical data was provided, along with higher recovery of the lesion where structural information was not available. The application of these hybrid techniques requires thorough evaluation of the order in which they should be applied and the defining of suitable parameters for their execution. The utility of these hybrid methods will be studied in the future.

6. Conclusion

In this paper an open-source toolbox for applying PVC to PET data has been presented. The toolkit provides an intuitive command-line interface to current techniques that can be incorporated into existing processing pipelines or used a basis for developing and evaluating novel PVC approaches. Each method implemented is capable of correcting for the tissue-fraction effect - a factor that is often overlooked. It is hoped the PETPVC toolbox will assist research in this field and encourage investigations into their clinical utility.

Acknowledgments

References

[1]   K. Erlandsson, I. Buvat, P. H. Pretorius, B. A. Thomas, and B. F. Hutton, "A review of partial volume correction techniques for emission tomography and their applications in neurology, cardiology and oncology," *Phys. Med. Biol.*, vol. 57, no. 21, p. R119, 2012.

[2]   K. Erlandsson, J. Dickson, S. Arridge, D. Atkinson, S. Ourselin, and B. F. Hutton, "Magnetic resonance imaging-guided partial volume correction of positron emission tomography data in PET / MRI," *PET Clin.*, p. epub ahead of print, 2016.

[3]   M. Soret, S. L. Bacharach, and I. Buvat, "Partial-volume effect in PET tumor imaging.," *J. Nucl. Med.*, vol. 48, no. 6, pp. 932–45, Jun. 2007.

[4]   B.-K. Teo, Y. Seo, S. L. Bacharach, J. a Carrasquillo, S. K. Libutti, H. Shukla, B. H. Hasegawa, R. a Hawkins, and B. L. Franc, "Partial-volume correction in PET: validation of an iterative postreconstruction method with phantom and patient data.," *J. Nucl. Med.*, vol. 48, no. 5, pp. 802–10, May 2007.

[5]   J. A. D. Aston, V. J. Cunningham, M.-C. Asselin, A. Hammers, A. C. Evans, and R. N. Gunn, "Positron emission tomography partial volume correction: estimation and algorithms.," *J. Cereb. Blood Flow Metab.*, vol. 22, no. 8, pp. 1019–34, Aug. 2002.

[6]   J. Yan, J. C.-S. Lim, and D. W. Townsend, "MRI-guided brain PET image filtering and partial volume correction," *Phys. Med. Biol.*, vol. 60, no. 3, pp. 961–976, Feb. 2015.

[7]   D. Yanase, I. Matsunari, K. Yajima, W. Chen, A. Fujikawa, S. Nishimura, H. Matsuda, and M. Yamada, "Brain FDG PET study of normal aging in Japanese: effect of atrophy correction.," *Eur. J. Nucl. Med. Mol. Imaging*, vol. 32, no. 7, pp. 794–805, Jul. 2005.

[8]   P. K. Curiati, J. H. Tamashiro-Duran, F. L. S. Duran, C. a. Buchpiguel, P. Squarzoni, D. C. Romano, H. Vallada, P. R. Menezes, M. Scazufca, G. F. Busatto, and T. C. T. F. Alves, "Age-related metabolic profiles in cognitively healthy elders: Results from a voxel-based [18F]fluorodeoxyglucose-positron-emission tomography study with partial volume effects correction," *Am. J. Neuroradiol.*, vol. 32, pp. 560–565, 2011.

[9]   Y. Su, T. M. Blazey, A. Z. Snyder, M. E. Raichle, D. S. Marcus, B. M. Ances, R. J. Bateman, N. J. Cairns, P. Aldea, L. Cash, J. J. Christensen, K. Friedrichsen, R. C.

Hornbeck, A. M. Farrar, C. J. Owen, R. Mayeux, A. M. Brickman, W. Klunk, J. C. Price, P. M. Thompson, B. Ghetti, A. J. Saykin, R. a Sperling, K. a Johnson, P. R. Schofield, V. Buckles, J. C. Morris, and T. L. S. Benzinger, "Partial Volume Correction in Quantitative Amyloid Imaging.," *Neuroimage*, vol. c, pp. 1–10, Dec. 2014.

[10]   B. F. Hutton, B. A. Thomas, K. Erlandsson, A. Bousse, A. Reilhac-Laborde, D. Kazantsev, S. Pedemonte, K. Vunckx, S. R. Arridge, and S. Ourselin, "What approach to brain partial volume correction is best for PET/MRI?," *Nucl. Instruments Methods Phys. Res. Sect. A Accel. Spectrometers, Detect. Assoc. Equip.*, 2012.

[11]   M. Quarantelli, K. Berkouk, A. Prinster, B. Landeau, C. Svarer, L. Balkay, B. Alfano, A. Brunetti, J.-C. Baron, and M. Salvatore, "Integrated software for the analysis of brain PET/SPECT studies with partial-volume-effect correction.," *J. Nucl. Med.*, vol. 45, no. 2, pp. 192–201, 2004.

[12]   O. G. Rousset, Y. Ma, and A. C. Evans, "Correction for Partial Volume Effects in PET: Principle and Validation," *J. Nucl. Med.* , vol. 39 , no. 5 , pp. 904–911, May 1998.

[13]   H. W. Muller-Gartner, J. M. Links, J. L. Prince, R. N. Bryan, E. McVeigh, J. P. Leal, C. Davatzikos, and J. J. Frost, "Measurement of Radiotracer Concentration in Brain Gray Matter Using Positron Emission Tomography: MRI-Based Correction for Partial Volume Effects," *J Cereb Blood Flow Metab*, vol. 12, no. 4, pp. 571–583, Jul. 1992.

[14]   M. Shidahara, C. Tsoumpas, A. Hammers, N. Boussion, D. Visvikis, T. Suhara, I. Kanno, and F. E. Turkheimer, "Functional and structural synergy for resolution recovery and partial volume correction in brain PET.," *Neuroimage*, vol. 44, no. 2, pp. 340–8, Jan. 2009.

[15]   D. B. Chonde, D. Izquierdo-Garcia, K. Chen, S. L. Bowen, and C. Catana, "Masamune: a tool for automatic dynamic PET data processing, image reconstruction and integrated PET/MRI data analysis," *EJNMMI Phys.*, vol. 1, no. Suppl 1, p. A57, 2014.

[16]   T. S. Yoo, M. J. Ackerman, W. E. Lorensen, W. Schroeder, V. Chalana, S. Aylward, D. Metaxas, and R. Whitaker, "Engineering and algorithm design for an image processing API: a technical report on ITK-the Insight Toolkit," *Stud. Health Technol. Inform.*, pp. 586–592, 2002.

[17]   C. Labbé, J. C. Froment, A. Kennedy, J. Ashburner, and L. Cinotti, "Positron Emission Tomography Metabolic Data Corrected for Cortical Atrophy Using Magnetic Resonance Imaging.," *Alzheimer Dis. Assoc. Disord.*, vol. 10, no. 3, 1996.

[18]   K. Erlandsson, A. T. Wong, R. van Heertum, J. J. Mann, and R. V. Parsey, "An improved method for voxel-based partial volume correction in PET and SPECT," *Neuroimage*, vol. 31, no. Supplement 2, p. T84, 2006.

[19]   B. A. Thomas, K. Erlandsson, M. Modat, L. Thurfjell, R. Vandenberghe, S. Ourselin, and B. F. Hutton, "The importance of appropriate partial volume correction for PET quantification in Alzheimer's disease.," *Eur. J. Nucl. Med. Mol. Imaging*, vol. 38, no. 6, pp. 1104–19, Jun. 2011.

[20] J. Yang, S. C. Huang, M. Mega, K. P. Lin, a. W. Toga, G. W. Small, and M. E. Phelps, "Investigation of partial volume correction methods for brain FDG PET studies," *IEEE Trans. Nucl. Sci.*, vol. 43, no. 6, pp. 3322–3327, 1996.

[21] J. Tohka and A. Reilhac, "Deconvolution-based partial volume correction in Raclopride-PET and Monte Carlo comparison to MR-based method.," *Neuroimage*, vol. 39, no. 4, pp. 1570–84, Feb. 2008.

[22] A. Fedorov, R. Beichel, J. Kalphaty-Cramer, J. Finet, J.-C. Fillion-Robbin, S. Pujol, C. Bauer, D. Jennings, F. Fennessy, M. Sonka, J. Buatti, S. Aylward, J. V. Miller, S. Pieper, and R. Kikinis, "3D Slicer as an Image Computing Platform for the Quantitative Imaging Network," *Magn. Reson. Imaging*, vol. 30, no. 9, pp. 1323–1341, 2012.

[23] I. Wolf, M. Vetter, I. Wegner, T. Böttger, M. Nolden, M. Schöbinger, M. Hastenteufel, T. Kunert, and H. P. Meinzer, "The medical imaging interaction toolkit," *Med. Image Anal.*, vol. 9, pp. 594–604, 2005.

[24] M. Nolden, S. Zelzer, A. Seitel, D. Wald, M. Müller, A. M. Franz, D. Maleike, M. Fangerau, M. Baumhauer, L. Maier-Hein, K. H. Maier-Hein, H. P. Meinzer, and I. Wolf, "The medical imaging interaction toolkit: Challenges and advances: 10 years of open-source development," *Int. J. Comput. Assist. Radiol. Surg.*, vol. 8, pp. 607–620, 2013.

[25] M. J. Cardoso, R. Wolz, M. Modat, N. Fox, D. Rueckert, and S. Ourselin, "Geodesic Information Flows," in *Medical Image Computing and Computer-Assisted Intervention – MICCAI 2012 SE - 33*, vol. 7511, N. Ayache, H. Delingette, P. Golland, and K. Mori, Eds. Springer Berlin Heidelberg, 2012, pp. 262–270.

[26] A. Reilhac, C. Lartizien, N. Costes, S. Sans, C. Comtat, R. N. Gunn, A. C. Evans, A. Monte, C. Pet, I. Terms, and M. Carlo, "PET-SORTEO : A Monte Carlo-Based Simulator With High Count Rate Capabilities," *IEEE Trans. Nucl. Sci.*, vol. 51, no. 1, pp. 46–52, 2004.
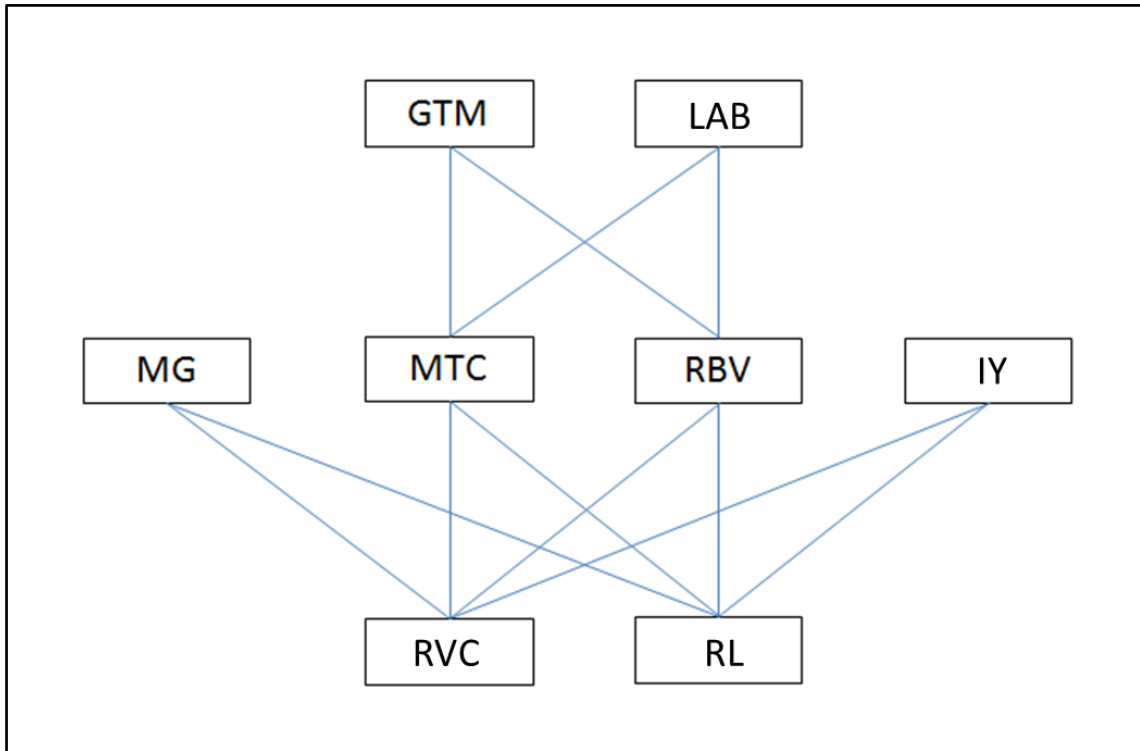
Figure 1. Twenty-two PVC techniques are included in the toolbox when combining the core methods. 1) GTM, 2) LAB, 3) MG, 4) MTC, 5) RBV, 6) IY, 7) RL, 8) RVC, 9) LAB-MTC, 10) LAB-RBV, 11) MG-RL, 12) MG-RVC, 13) MTC-RL, 14) MTC-RVC, 15) RBV-RL, 16) RBV-RVC, 17) IY-RL, 18) IY-RVC, 19) LAB-MTC-RL, 20) LAB-MTC-RVC, 21) LAB-RBV-RL, 22) LAB-RBV-RVC.
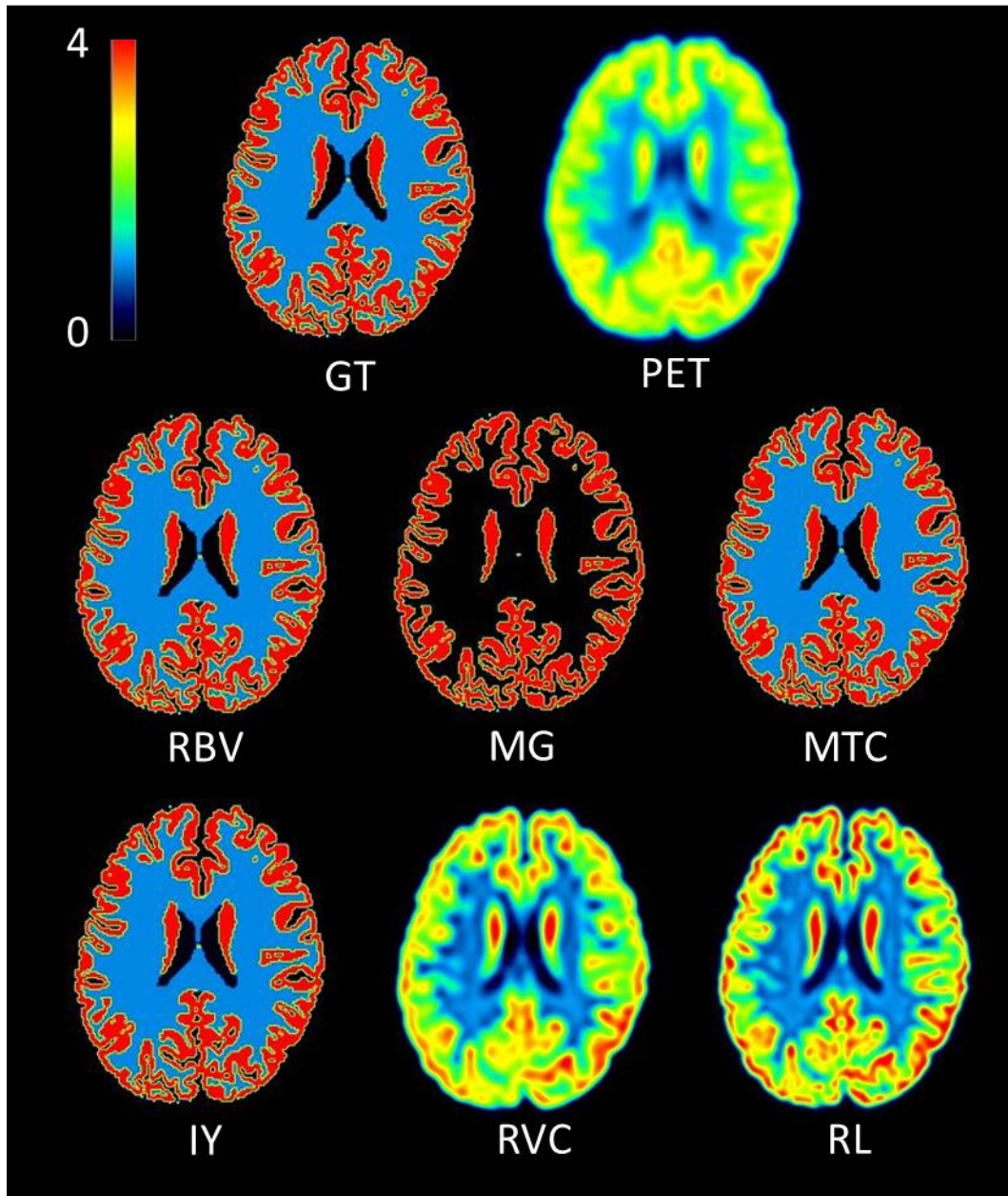
Figure 2. Trans-axial images before and after PVC. The ground truth (GT) and simulated FDG PET data (PET) (top), images corrected using RBV, MG and MTC (middle) and with IY, RVC and RL (bottom).
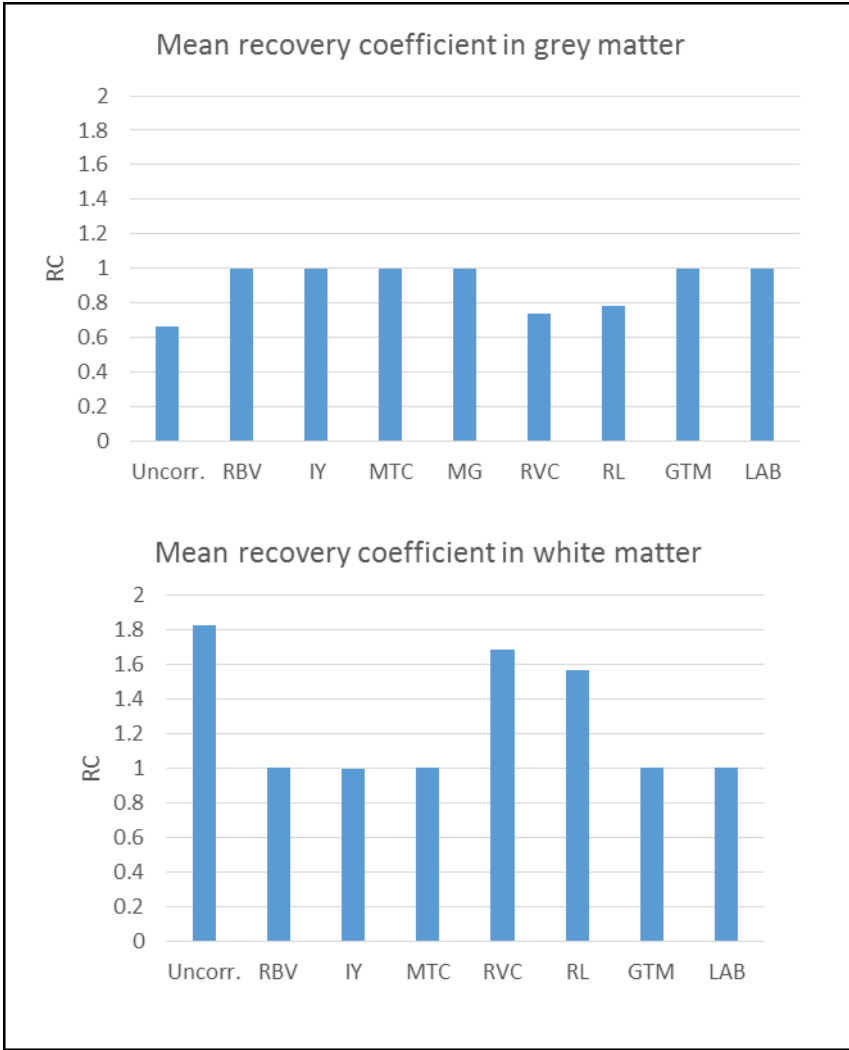
Figure 3. The mean recovery coefficient (RC) for the uncorrected (Uncorr.) and PV-corrected grey matter (top row) and white matter (bottom row). Note the white matter RC value is not given for the MG correction as it does not correct this compartment.
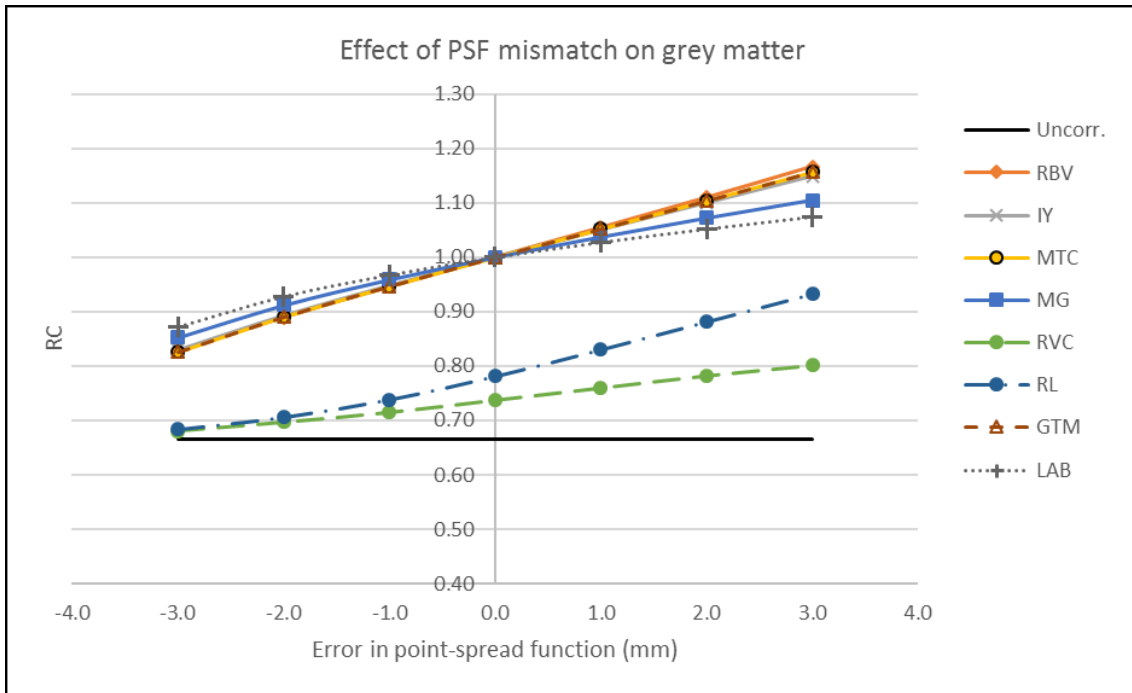
Figure 4. The effect of applying the incorrect (±3mm) point-spread function (PSF) estimate during PVC. The RC of the uncorrected PET (Uncorr.) is shown for reference purposes with a solid black line.
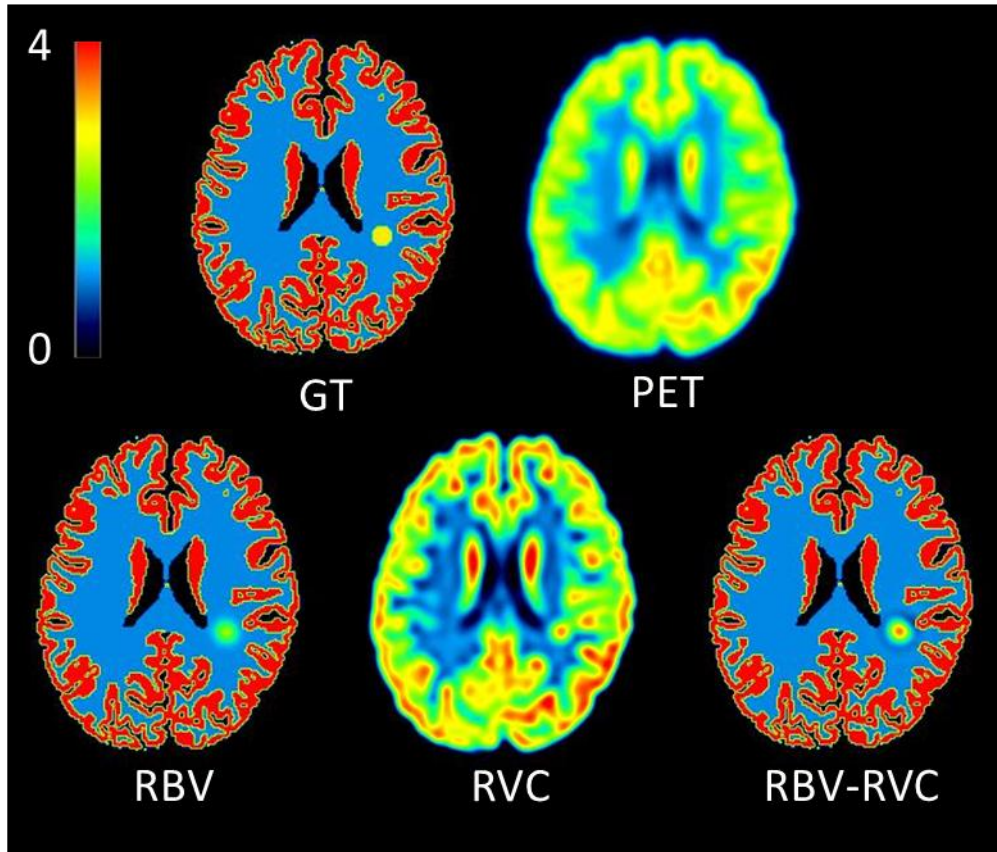
Figure 5. Trans-axial images with added lesion before and after partial volume correction. The ground truth (GT) and simulated FDG PET data (PET) (top), images corrected using RBV, RVC and RBV-RVC (bottom).
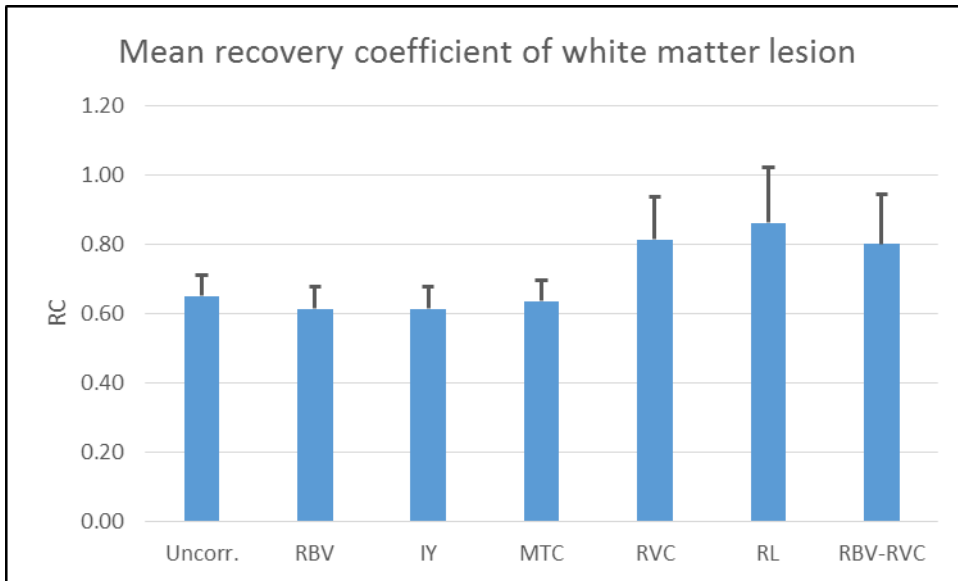
Figure 6. The mean recovery coefficient (RC) for the uncorrected (Uncorr.) and PV-corrected

WM lesion. Error bars represent one standard deviation.
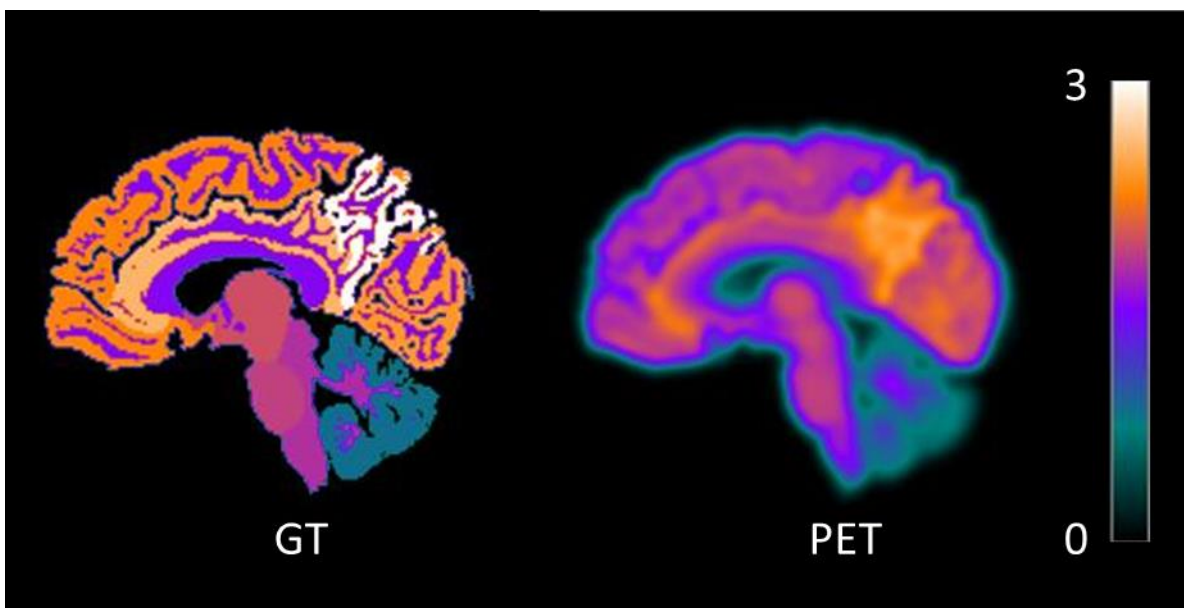
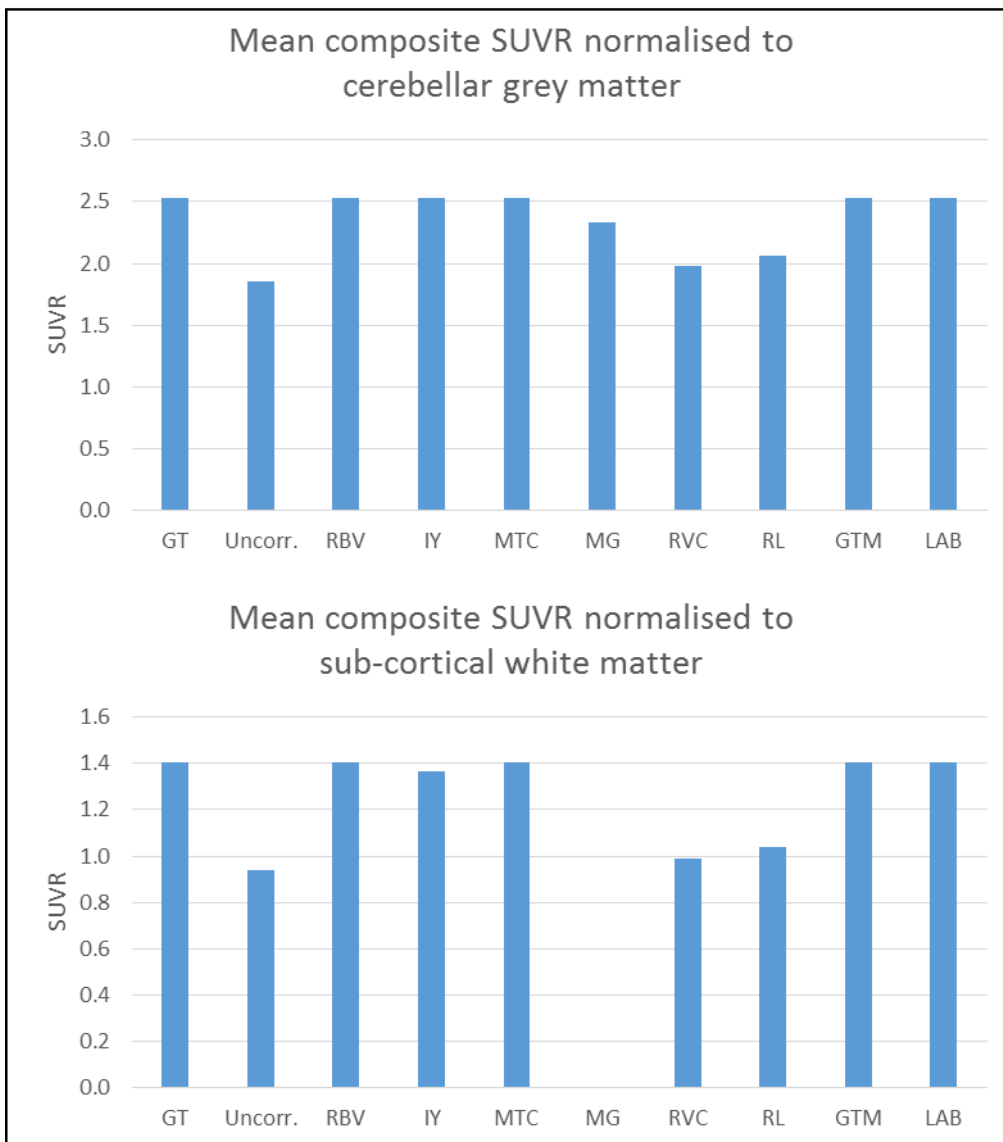Figure 7. Sagittal slices of the PIB ground truth (GT) and simulated noise-free PET image.

Figure 8. Mean composite cortical SUVRs of the noise-free PIB simulation, normalised to cerebellar grey matter (top) and sub-cortical white matter (bottom). The SUVR for MG-corrected sub-cortical white matter normalisation is not shown as the technique does not correct for white matter regions.
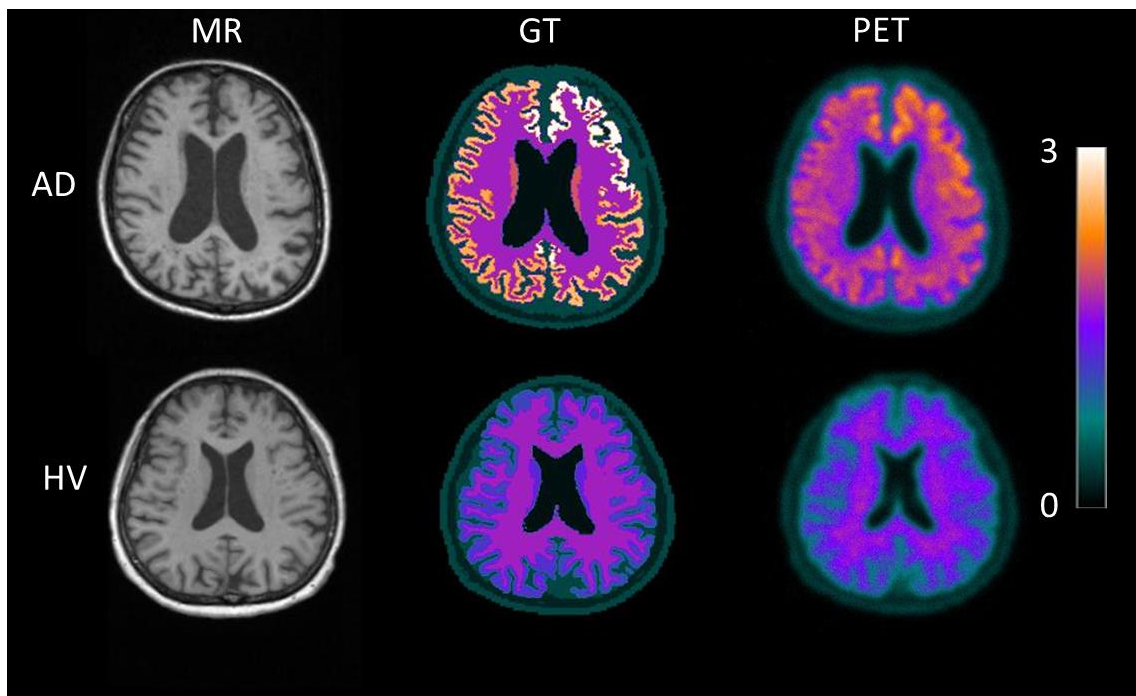
Figure 9. MP-RAGE MR images (left), PIB distribution ground truth (GT; middle) and simulated PET data (right). Top row represents an AD subject. Bottom row represents a healthy volunteer (HV). GT and PET are SUVR images, normalised to cerebellar GM.
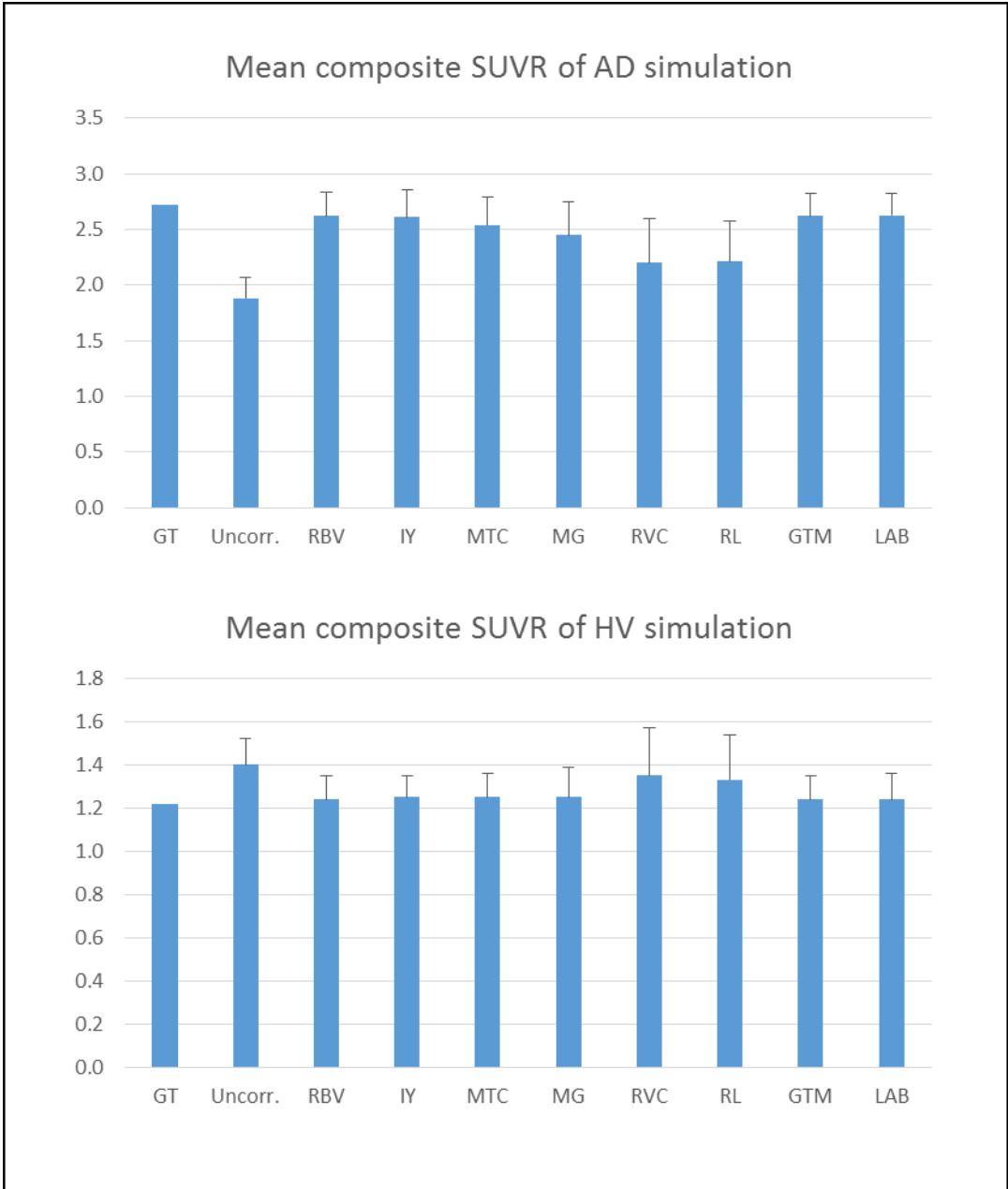
Figure 10. Mean composite cortical SUVRs of the Monte Carlo PIB simulations of an AD subject (top) and healthy volunteer (bottom). Error bars represent the standard deviation across noise realisations.